NCAR Manuscript No. 259a

Nonlinear Shallow Fluid Flow Over an Isolated Ridge

by

David D. Houghton and Akira Kasahara

National Center for Atmospheric Research

Boulder, Colorado

January 1967

Abstract

The shallow water theory is applied to the study of one dimensional fluid flows over an isolated ridge. The work was motivated by the desire to investigate the phenomenon called the chinook which occurs on the eastern side of the Rockies and is characterized by extremely strong winds which blow from the mountains.

The motion that arises from an initially uniform flow involves the formation of hydraulic jumps both on the windward and leeward sides of a ridge. Special emphasis is put on determining analytically the asymptotic structure of such flows with jumps by solving the appropriate "steady" state equations. The presence of the hydraulic jumps and a rarefaction wave was revealed by preliminary numerical solutions of the time dependent problems.

These numerical results demonstrate the evolution in time of the various features of the flow found in the asymptotic solutions.

1. Introduction

Areas along the eastern slope of the Rocky Mountains are struck from time to time during winter and spring by strong and relatively warm winds which suddenly flow down from the mountains. This phenomenon is known as the chinook (the North American counterpart of the European foehn) and occurs on the eastern side of the Rockies. Very few synoptic investigations have been made concerning the weather conditions at the time of typical chinook events in the Rocky Mountain area and therefore the cause of the chinook in this particular area is still not well known (see [9]). Similar phenomena are frequently observed in the Owens Valley located on the eastern side of the Sierra Nevadas (see [5]).

Concerning airflow over mountains, much literature is available ranging from purely theoretical studies on mountain waves to case studies of the synoptic weather conditions at the time of strong winds (e.g., see [1]). The theoretical studies mostly use linear perturbation methods, and very little work has been done on nonlinear aspects. One of the drawbacks of using linearized theories in this respect is that we miss the phenomenon of the "hydraulic jump," which can arise only from nonlinear equations. In fact, Kuettner [6] attempted to apply the concept of "jump" in hydraulics to explain the appearance of rotor clouds in the lee of mountains.

In this study we investigate the nature of the hydraulic jumps in flows across a ridge. We use the one-dimensional time-dependent "shallow water" equations that govern the motion of an incompressible, homogeneous,

inviscid, and hydrostatic fluid. This model gives a crude representation of atmospheric flow, but it corresponds very closely to laboratory experiments carried out by Long [8]. In his experiments an obstacle was drawn by a motor drive at a uniform speed along the bottom of a channel filled with water and the occurrence of hydraulic jumps in the fluid was demonstrated for a certain range of velocities of the obstacle.

In the present study the asymptotic mathematical solutions to the model equations are determined for the case where the fluid initially at rest is impulsively accelerated to a velocity which is constant in the space coordinate. In Section 2 the basic equations are described. In Section 3 the criteria for the formation of hydraulic jumps are derived and the structure of the jumps is determined by using steady state equations together with hydraulic jump conditions. In Section 4 the corresponding time-dependent equations are solved numerically and the results are favorably compared with the analytical solutions.

2. Basic equations

We consider one-dimensional "shallow water" flow over an isolated obstacle as shown in Fig. 1. The governing equations may be written as (see [10]),

$$\frac{\partial u}{\partial t} + u\frac{\partial u}{\partial x} + g\frac{\partial \varphi}{\partial x} + g\frac{\partial H}{\partial x} = 0 \ , \tag{2.1a}$$

$$\frac{\partial \varphi}{\partial t} + \frac{\partial}{\partial x}(\varphi u) = 0 \ , \tag{2.1b}$$

where x and t denote the space and time coordinates which are independent variables; u and φ denote the horizontal velocity and the depth of the fluid; H is the height of an obstacle which is a function of x. The lower boundary is flat and horizontal except where the obstacle exists. The parameter g denotes the vertical acceleration due to gravity.

We consider the following problem. For $t < 0$ and $-\infty < x < \infty$, the fluid is completely at rest and the height of the free surface is constant, i.e., no pressure gradients exist. We denote this initial height by h_o. At $t = 0$ the fluid is impulsively set in motion so that for $-\infty < x < \infty$ it has a constant horizontal velocity u_o. The problem is then to determine the subsequent motion of the fluid.

3. Asymptotic solutions

From such an impulsive start, it is expected that a transient motion develops at the obstacle and moves out to infinity in both directions. After sufficient time has elapsed, the solution in the neighborhood of the obstacle should then be determined by an analysis of the steady state solutions of equations (2.1). We refer to this solution of an initial value problem as an asymptotic solution rather than merely a steady state solution.

The system of equations (2.1) admits the following steady state solutions for u and φ:

$$\frac{u^2}{2g} + \varphi + H = K_1 = \text{const.}, \tag{3.1a}$$

$$\varphi u = K_2 = \text{const.} \tag{3.1b}$$

If a continuous flow is considered, i.e., without hydraulic jumps, the two constants K_1 and K_2 are determined by the velocity u_o and the height h_o of the approaching flow far from the obstacle. Thus,

$$K_1 = \frac{u_o^2}{2g} + h_o \qquad \text{and} \qquad K_2 = u_o h_o \,. \tag{3.2}$$

Eliminating φ from (3.1a) by using (3.1b) and introducing the dimensionless parameters F_o and M, and the dimensionless variable U by

$$F_o \equiv \frac{u_o}{\sqrt{gh_o}} , \qquad M \equiv \frac{H}{h_o} , \qquad U \equiv \frac{u}{u_o} , \tag{3.3}$$

we obtain

$$\frac{F_o^2}{2} U^3 + U\left(M - \frac{F_o^2}{2} - 1\right) + 1 = 0 . \tag{3.4}$$

Note that the quantity M is a function of x, but it is considered here as a parameter. There exist (see Figures 2a,b) three real roots of (3.4) for $M < M_*$, and if the condition

$$M = M_* \equiv \frac{F_o^2}{2} - \frac{3}{2} F_o^{2/3} + 1 \tag{3.5}$$[1]

---

[1] The condition (3.5) was also discussed by Long [8] and Chao, Chang, and Yan [3].

---

is satisfied, then two of these roots are equal to

$$U_* \equiv F_o^{-2/3} .$$

For convenience of presentation, we consider a smooth convex obstacle which is symmetric with respect to its crest, e.g. as is shown in Fig. 1. To represent the height of the obstacle, we use the parameter M_c indicating the ratio of the height of the crest H_c over the depth of the approaching fluid h_o,

$$M_c = \frac{H_c}{h_o} . \qquad (3.6)$$

Fig. 3 shows the curve of Eq. (3.5) plotted with $M_c = M_*$ as the abscissa and F_o as the ordinate. In domain I below the lower curve and domain III above the upper curve, i.e., the regions characterized by $M_c < M_*$, there is only one real solution of (3.4) which is physically meaningful, as explained below. Fig. 2a shows the root U(x) of the cubic equation (3.4) which varies continuously with M(x) for a particular value of $F_o < 1$. Fig. 2b shows the same for a particular value $F_o > 1$. If $F_o < 1$, as shown in Fig. 2a, the physically meaningful root begins at $U(-\infty) = 1$ for $M(-\infty) = 0$ and increases to a value $U_c < U_*$ as M increases to $M_c < M_*$. U(x) then decreases to $U(+\infty) = 1$ as M decreases to $M(+\infty) = 0$. If $F_o > 1$, as shown in Fig. 2b, the physically meaningful root begins at $U(-\infty) = 1$ for $M(-\infty) = 0$ and decreases to a value $U_c > U_*$ as M increases to $M_c < M_*$. U(x) then increases to $U(+\infty) = 1$ as M decreases to $M(+\infty) = 0$. The case $F_o = 1$ is a degenerate case for which no steady solution occurs with an obstacle ~~jump~~ present ~~occurs~~. In domain II, $M_c > M_*$ and no physically meaningful solution exists, as seen from Fig. 2a,b.

The flows characterized by the parameters F_o and M_c in domain I in Fig. 3 are everywhere subcritical and the free surface of the steady states dips symmetrically over the symmetrical obstacle. On the other hand, the flows in domain III are everywhere supercritical and the free surface of the steady states rises symmetrically over the obstacle.

It was shown by Long [8] that the flow with parameters F_o and M_c in domain II must become discontinuous. He then discussed qualitatively the nature of the flow with jumps. In the following, we shall discuss in detail the structure of the flow with hydraulic jumps.

If the condition $M = M_*$ is met at some point over the obstacle, let us denote the corresponding velocity and depth by u_* and φ_*. Then, it can be shown from (3.1) and (3.2) that

$$u_* = \sqrt{g\varphi_*} \ . \tag{3.7}$$

In other words, the flow speed becomes "sonic" or "critical" when the condition (3.5) is satisfied. (It is well known that the "characteristics" of equation (2.1) are $dx/dt = u \pm \sqrt{g\varphi}$.) It can be shown that this critical condition occurs at the obstacle crest for the flow with parameters F_o and M_c in domain II.

In order to study a discontinuity that may develop on the windward side, let us consider a situation in which the obstacle is high enough, so that the obstacle acts to partially block the flow and a bore forms and propagates upstream as shown in Fig. 4. We let h_A and u_A denote the steady state height and the velocity of the fluid behind the bore, c_ℓ the propagation velocity of the bore, and φ_c and u_c the fluid depth and velocity at the obstacle crest. Here we have five unknowns: h_A, u_A, u_c, φ_c, and c_ℓ. Therefore, five equations are needed to determine the structure of the flow for given H_c, h_o, and u_o. The two jump conditions at the bore are expressed by

$$c_\ell = \frac{h_o u_o - h_A u_A}{h_o - h_A} \tag{3.8}$$

and

$$c_\ell = u_o - \sqrt{\frac{g h_A}{h_o}\left(\frac{h_A + h_o}{2}\right)} \quad . \tag{3.9}$$

Condition (3.8) is based on the conservation of mass relative to the bore and (3.9) is based on the conservation of momentum across the bore as discussed in detail by Stoker [10]. These two shock conditions can also be derived mathematically from the system of conservation equations (4.1) by applying the theory of weak solutions (see Courant [4]). The three other equations are the two steady state conditions given in (3.1a,b) and the critical condition given by (3.7). That is, from Figures 2a,b, in order to find an asymmetric continuous "steady" solution for say U(x) over the obstacle, we must require that $M_c = M_A$, where M_A is given by the right-hand side of (3.5) with F_o replaced by $\mathcal{F}_A = u_A/\sqrt{g h_A}$. Thus, we have

$$\frac{u_c^2}{2g} + \varphi_c + H_c = \frac{u_A^2}{2g} + h_A \equiv K_3 \ , \tag{3.10}$$

$$u_c \varphi_c = u_A h_A \equiv K_4 \ , \tag{3.11}$$

$$u_c = \sqrt{g\varphi_c} \ , \tag{3.12}$$

where K_3 and K_4 are constants different from K_1 and K_2. For given values of H_c, h_o, and u_o, the five unknowns are determined by solving (3.8) through (3.12).

It can be shown that the upstream jump always propagates away from the obstacle because $\overset{h}{u}_A u_A < h_o u_o$ and $h_A > h_o$. Furthermore, it follows that the flow in the steady state region upstream of the obstacle crest is always subcritical.

At the crest the flow is critical as mentioned earlier. If the flow on the lee side is assumed to be subcritical, then the solution is symmetrical and it can be shown that such a physically meaningful flow structure does not exist downstream. Thus we choose the supercritical branch ($U > U_*$) of Figure 2a to represent the asymmetrical steady state condition on the lee side of the obstacle crest and try to determine an asymptotic solution downstream of the obstacle. It is reasonable to assume that, corresponding to the upstream side, the steady state conditions over the obstacle extend down the lee side to create a new steady depth h_B and velocity u_B as indicated in Fig. 5. These can be determined from the two steady state conditions

$$\frac{u_B^2}{2g} + h_B = K_3 \ , \tag{3.13}$$

$$u_B h_B = K_4 \ , \tag{3.14}$$

subject to the asymmetrical requirement of $h_B \neq h_A$ and $u_B \neq u_A$. The constants K_3 and K_4 are already given by (3.10) and (3.11).

The remaining problem is to describe the transition between the newly determined steady state given by u_B and h_B and the downstream initial state further away from the obstacle given by u_o and h_o which is identical to the upstream initial conditions. We consider the simplest possible ways to describe the transition. If only a hydraulic jump is assumed, then one new variable c_r, the propagation velocity of the jump, is introduced. However, two additional jump conditions must be satisfied and therefore the problem becomes overdetermined mathematically. Similarly if only a rarefaction wave is assumed, no new variable is introduced but only one condition for the rarefaction wave, say $u - 2\sqrt{gh} = \text{constant}$, must be satisfied and the problem again becomes overdetermined. The problem is well posed if both a hydraulic jump and a rarefaction wave are assumed as shown in Fig. 5. Since there are three conditions to be satisfied, we introduce two additional variables h_X and u_X besides the propagation velocity of the jump c_r.

Thus the three remaining unknowns u_X, h_X, and c_r are determined from the two jump conditions

$$c_r = \frac{h_B u_B - h_X u_X}{h_B - h_X}, \tag{3.15}$$

$$c_r = u_B - \sqrt{\frac{gh_X}{h_B}\,\frac{h_X + h_B}{2}}\,, \tag{3.16}$$

and the rarefaction wave condition

$$u_X - 2\sqrt{gh_X} = u_o - 2\sqrt{gh_o} \tag{3.17}$$

where u_B, h_B, u_o, and h_o are given.

The ten equations (3.8) through (3.17) determine uniquely the ten variables c_ℓ, h_A, u_A, u_c, φ_c, h_B, u_B, c_r, h_X, and u_X which represent the asymptotic solution of the flow in domain II of Fig. 3. The values of these ten variables are determined as functions of the Froude number, F_o, of the initial flow and the dimensionless height of the crest of the obstacle, M_c. For convenience of presentation, we introduce the following dimensionless variables:

$$\mathcal{F}_A = \frac{u_A}{c_o}\,, \qquad \mathcal{F}_B = \frac{u_B}{c_o}\,, \qquad \mathcal{F}_X = \frac{u_X}{c_o}\,,$$

$$D_A = \frac{h_A}{h_o}\,, \qquad D_B = \frac{h_B}{h_o}\,, \qquad D_X = \frac{h_X}{h_o}\,, \tag{3.18}$$

$$C_i = \frac{c_\ell}{c_o}\,, \qquad C_r = \frac{c_r}{c_o}\,,$$

$$\Phi_c = \frac{\varphi_c}{h_o}\,, \qquad \mathcal{F}_c = \frac{u_c}{c_o}\,,$$

where

$$c_o = \sqrt{gh_o} \ .$$

In Fig. 6, contour plots of the values of D_A and $\mathcal{F}_A$ are shown by the solid and dashed lines respectively. The solutions are shown for domain II as defined in Fig. 3. Thus, the heavy solid curve enclosing the group of lines is the critical curve shown in Fig. 3. The region below the dashed line for $\mathcal{F}_A = 0$ is where a total blockage of the flow occurs. Along the dashed line for $\mathcal{F}_A = 0$ the maximum height of the obstacle is larger than the depth of the initial flow h_o and the flow is blocked completely, namely $u_A = 0$ and $h_A = H_c$. If we substitute these two conditions in (3.8) and (3.9), and then equate these two equations, we obtain

$$\frac{h_o u_o}{h_o - H_c} = u_o - \sqrt{\frac{gH_c}{h_o}\left(\frac{H_c + h_o}{2}\right)}$$

or using the definitions of M_c and F_o, the above equation may be written as

$$F_o = \left(\frac{M_c - 1}{M_c}\right)\sqrt{M_c\left(\frac{1 + M_c}{2}\right)} \ . \qquad (3.19)$$

The dashed line for $\mathcal{F}_A = 0$ is drawn based on the relationship (3.19).

Fig. 7 shows the contour lines of the quantity C_ℓ. The negative values of C_ℓ denote that the bore propagates in the upstream direction, as already discussed. Fig. 8 exhibits the contour lines of Φ_c and $\mathcal{F}_c$ by solid and dashed lines, respectively. Fig. 9 gives the contour lines of C_r by solid lines. Along the heavy dashed line representing the curve of $C_r = 0$, the lee jump remains stationary. In the remaining part of domain II below the curve for $C_r = 0$, the solution of C_r shows negative values (which, however, are not presented here). This implies that the lee jump never propagates off the obstacle, and the downstream configuration shown in Fig. 5 cannot exist. Hereafter the upper part of domain II where the lee jump moves will be denoted by IIb. The remaining lower part will be denoted by IIa. In Fig. 3 the dashed line separates these two parts of domain II.

In domain IIa we therefore seek another configuration, as shown in Fig. 10. That is, we now investigate the conditions under which the lee jump remains stationary on the <u>downstream side of the obstacle crest</u>. We denote by φ_- and u_- the depth and velocity on the upstream side of the lee jump and φ_+ and u_+ the depth and velocity on the downstream side, as shown in Fig. 10. Since the jump is stationary, we have the conditions

$$c_r = \frac{\varphi_- u_- - \varphi_+ u_+}{\varphi_- - \varphi_+} = 0 \ , \tag{3.20}$$

$$c_r = u_- - \sqrt{\frac{g\varphi_+}{\varphi_-}\left(\frac{\varphi_+ + \varphi_-}{2}\right)} = 0 \ . \tag{3.21}$$

There are seven unknowns: u_+, u_-, φ_+, φ_-, h_x, u_x, and H^*. The last unknown, H^*, is the height of the obstacle where the stationary jump stays. These unknowns are determined by solving seven equations, including (3.20) and (3.21). The other five equations are the steady state conditions from the windward side of the obstacle to the upstream side of the lee jump,

$$h_A u_A = \varphi_- u_- \ , \tag{3.22}$$

$$\frac{u_A^2}{2g} + h_A = \frac{u_-^2}{2g} + \varphi_- + H^* \ , \tag{3.23}$$

and the steady state conditions from the downstream side of the lee jump to the region off the downstream side of the obstacle:

$$h_x u_x = \varphi_+ u_+ \ , \tag{3.24}$$

$$\frac{u_x^2}{2g} + h_x = \frac{u_+^2}{2g} + \varphi_+ + H^* \ . \tag{3.25}$$

The remaining equation is the rarefaction wave condition which is identical to (3.17),

$$u_o - 2\sqrt{gh_o} = u_x - 2\sqrt{gh_x} \quad . \tag{3.26}$$

Let us introduce the dimensionless variables defined by

$$\Phi_+ = \frac{\varphi_+}{h_o} , \qquad \Phi_- = \frac{\varphi_-}{h_o} ,$$

$$\mathcal{F}_+ = \frac{u_+}{c_o} , \qquad \mathcal{F}_- = \frac{u_-}{c_o} , \tag{3.27}$$

$$M^* = \frac{H^*}{h_o} \quad .$$

The values of H^* are indicated in Fig. 9 by the dashed contour lines of M^*. On the curve of $C_r = 0$, it is seen that $M^* = 0$, i.e., the lee jump is stationary at the very edge of the obstacle. Fig. 11 gives the contour lines of D_x and $\mathcal{F}_x$ as solid and dashed lines, respectively. In domain IIa, the contour lines of D_x and $\mathcal{F}_x$ obtained from Eqs. (3.20) - (3.26) are shown. In domain IIb the contour lines of D_x and $\mathcal{F}_x$ obtained from Eqs. (3.8) - (3.17) are presented. Fig. 12 shows the contour lines of D_B and $\mathcal{F}_B$ in domain IIb and those of Φ_- and $\mathcal{F}_-$ in domain IIa. Note that the contour lines of D_B join continuously to those of Φ_- and that the contour lines of $\mathcal{F}_B$ join continuously to those of $\mathcal{F}_-$ at the transition curve between domains IIa and IIb. Finally, Fig. 13 exhibits the contour lines of Φ_+ and $\mathcal{F}_+$ which exist only in domain IIa.

4. Numerical solutions

In this section we describe the numerical integration scheme for the time-dependent equations (2.1a,b) and the numerical results obtained in certain illustrative examples. After a sufficiently long time, the numerical solutions approach the asymptotic states which were discussed in the previous section. We used a numerical scheme developed by Lax and Wendroff [7] which is suited to handle discontinuous solutions. Since the derivation of the two jump conditions (3.8) and (3.9) assumes the conservation of momentum and mass, the numerical computation should be performed on the system of equations which conserves momentum and mass (see for example Burstein [2]). (In as yet unpublished work, H. O. Kreiss gives a more complete development of such methods and shows that for a large class of schemes the conservation form of the equations is not a prerequisite for the accurate calculation of discontinuous solutions.)

Let us, then, rewrite Eqs. (2.1a,b) in the form,

$$\frac{\partial W}{\partial t} + \frac{\partial G}{\partial x} + K = 0 \tag{4.1}$$

where

$$W = \begin{pmatrix} m \\ \varphi \end{pmatrix} , \qquad G = \begin{pmatrix} \frac{m^2}{\varphi} + g\frac{\varphi^2}{2} \\ m \end{pmatrix} ,$$

$$K = \begin{pmatrix} g\varphi \frac{\partial H}{\partial x} \\ 0 \end{pmatrix} , \qquad m = \varphi u . \tag{4.2}$$

If we let Δt be the time increment and expand $W(x,t + \Delta t)$ in a Taylor series in time, we have

$$W(x,t + \Delta t) = W(x,t) + \Delta t \frac{\partial W}{\partial t} + \frac{1}{2} (\Delta t)^2 \frac{\partial^2 W}{\partial t^2} + O(\Delta t^3) ,$$

where the time derivatives are evaluated at time t. To insure second order accuracy in Δt, it is necessary to retain the second order term. By using (4.1), the time derivatives in the Taylor series can be replaced by space derivatives to give

$$W(x,t + \Delta t) \doteq W(x,t) - \Delta t \left(\frac{\partial G}{\partial x} + K \right) + \frac{(\Delta t)^2}{2} \left\{ \frac{\partial}{\partial x} \left[A \left(\frac{\partial G}{\partial x} + K \right) \right] - \frac{\partial K}{\partial t} \right\} , \tag{4.3}$$

where

$$A = \begin{pmatrix} \frac{2m}{\varphi} , & g\varphi - \frac{m^2}{\varphi^2} \\ 1 & 0 \end{pmatrix} , \qquad \frac{\partial K}{\partial t} = \begin{pmatrix} -g \frac{\partial m}{\partial x} \frac{\partial H}{\partial x} \\ 0 \end{pmatrix} .$$

We then approximate the space derivatives by centered differencing schemes to secure second order accuracy in the space increment, Δx, as well as in Δt. Let us denote $W(x,t)$ for $x = j\Delta x$ and $t = \ell\Delta t$ by W_j^{ℓ}. The finite difference equation of (4.3) may then be written as

$$W_j^{\ell+1} = W_j^{\ell} - \lambda[\Delta' G_j^{\ell} + K_j^{\ell}]$$

$$+ \frac{\lambda^2}{2} \left[\bar{A}_{j+\frac{1}{2}}^{\ell} \{\Delta G_{j+\frac{1}{2}}^{\ell} + K_{j+\frac{1}{2}}^{\ell}\} \right. \tag{4.4}$$

$$\left. - \bar{A}_{j-\frac{1}{2}}^{\ell} \{\Delta G_{j-\frac{1}{2}}^{\ell} + K_{j-\frac{1}{2}}^{\ell}\} + Q_j^{\ell} \right]$$

where

$$\lambda = \frac{\Delta t}{\Delta x}$$

$$\Delta_{j+\frac{1}{2}} = (\quad)_{j+1} - (\quad)_j$$

$$\Delta'_j = \frac{1}{2}\{(\quad)_{j+1} - (\quad)_{j-1}\}$$

$$\overline{(\quad)}_{j+\frac{1}{2}} = \frac{1}{2}\{(\quad)_{j+1} + (\quad)_j\}$$

$$K_j^{\ell} = \begin{pmatrix} g\varphi_j^{\ell} \cdot \Delta' H_j \\ 0 \end{pmatrix}$$

$$K_{j+\frac{1}{2}}^{\ell} = \begin{pmatrix} g\bar{\varphi}_{j+\frac{1}{2}}^{\ell} \cdot \Delta H_{j+\frac{1}{2}} \\ 0 \end{pmatrix}, \qquad Q_j^{\ell} = \begin{pmatrix} g\Delta' H_j \cdot \Delta' m_j^{\ell} \\ \end{pmatrix}.$$

It has been shown by Lax and Wendroff [7] that stability of the scheme is insured if λ satisfies the condition

$$R_m = \lambda\,(u_m + \sqrt{gh_m}) \;< 1 \tag{4.5}$$

where u_m is the largest possible flow speed and h_m is the maximum height of the free surface of the flow. It was found, as is well known, that

oscillations in the vicinity of jumps and discontinuities at the obstacle crest were suppressed if the ratio λ were made as large as possible.

We centered the obstacle at the origin of the x coordinate. The form of the obstacle was given by

$$H(x) = H_c(1 - x^2/a^2) \qquad \text{for } 0 \le |x| \le a$$

$$= 0 \qquad \text{for } |x| > a$$

where H_c is the height of the crest.

We selected the dimensional values for the parameters of the problem in such a way that the numerical results could be compared easily and qualitatively with those of laboratory experiments conducted by Long [8].

$h_o = 20$ cm

$a = 40\ \Delta x$

$L = 1000\ \Delta x$

$\Delta x = 1.0$ cm

$g = 980$ cm/sec^2

The initial conditions were $u = u_o$ and $\varphi = h_o - H$ for $-L < x < L$ at $t = 0$. The constant u_o varied from case to case. The boundary conditions in x were chosen to be periodic, that is, $u(L) = u(-L)$ and

$\varphi(L) = \varphi(-L)$. These boundaries at $x = \pm L$ are set sufficiently distant from the obstacle so that the asymptotic conditions are well established in the vicinity of the obstacle before wave motions can be fed back into this region by the periodic boundary conditions.

Numerical solutions were obtained to illustrate the various features of the flow found in the analytical solutions: the subcritical symmetrical conditions in domain I, the stationary lee jump in domain IIa, the downstream moving lee jump in domain IIb, and the supercritical symmetrical conditions in domain III. These were obtained by selecting $M_c = .5$ and $F_o = .2$, .3, .7, and 1.9, respectively. These cases, labeled A,B,C, and D, are shown by the crossed circles in Fig. 3.

Fig. 14a shows the numerical solution of Case A after 1000 time steps representing 4.6 seconds for the dimensional parameters given, where $R_o = .77$. (R_o is given by Eq. (4.5) with u_m and h_m replaced by the initial values u_o and h_o.) Similarly Figs. 14b,c,d show the numerical solutions in Cases B, C, and D after 400, 400, and 1000 time steps representing 1.8, 1.4, 2.3 seconds of real time, respectively. In Cases B, C, D, the quantity ΛR_o equals .83, .82, and .93, respectively. The figures show the solution as it was plotted directly by the computer on a dd80 digital display unit. Only 500 of the total 2000 spatial grid points are shown in each diagram.

The numerical results clearly confirm the conclusions of the analytical study concerning the evolution of the flow in each of the

domains. The transient gravity waves that are generated by the mountain and the impulsive initial flow are not evident in Case A as they have passed from the vicinity of the mountain. In Case D, which is supercritical, part of one of the gravity waves of the transient solution is still visible at the right side. In Cases B and C the transient solutions are buried in the features of the asymptotic solution. For example, the downstream moving wave moves with the downstream rarefaction wave. In three of the figures the position of a fluid particle originating over the obstacle crest at $t = 0$ and moving with the local fluid velocity u is shown by a small flying arrow.

These numerical results agree quite accurately with the asymptotic features described in Section 3 (see Table 1). In Cases A and D the numerical errors in certain quantities are less than .1%. In Cases B and C the numerical errors are less than 2% for all the asymptotic values that can be evaluated accurately. In Case B some values were evaluated at the lee jump and the oscillations in the finite difference solution there, due to truncation errors, prevented an accurate determination of these values.

Table I

Summary of Numerical Results

Case	A		B		C		D	
Asymptotic Quantity	Analytical Value	Computed Value	Analytical Value	Computed Value	Analytical Value	Computed Value	Analytical Value	Computed Value
D_A			1.0672	1.0671	1.3677	1.3676		
$\mathcal{F}_A$			0.2338	0.2339	0.3579	0.3580		
C_ℓ			-0.7503	-0.782	-0.5724	-0.569		
Φ_c	0.3852	0.3856	0.3964	0.3964	0.6211	0.6211	1.4722	1.472
$\mathcal{F}_c$	0.5192	0.5187	0.6296	0.6295	0.7881	0.7883	1.2905	1.290
C_r					0.1541	0.15		
M^*			0.2915	0.3				
D_B					0.3298	0.3298		
$\mathcal{F}_B$					1.4846	1.4846		
Φ_-			0.2339	0.2				
$\mathcal{F}_-$			1.0669	1.				
Φ_+			0.6221	0.6				
$\mathcal{F}_+$			0.4012	0.4				
D_x			0.9603	0.9603	0.9281	0.928		
$\mathcal{F}_x$			0.2599	0.2599	0.6268	0.628		

5. Conclusions

The shallow water theory was applied to an investigation of fluid flows over an isolated ridge. The results of the analytical study reveal that there are three classes of motion in the parameter domain of F_o and M_c as shown in Fig. 3. In domain I, the motions are subcritical and steady states exist over the ridge without jumps. In domain III, the motions are supercritical and steady states exist over the ridge without jumps. In domain II, the steady state solutions exist only with accompanying jumps on both sides of the ridge. The jump on the windward side of the ridge always moves upstream. The jump on the lee side moves downstream in domain IIb and remains stationary over the lee slope of the ridge in domain IIa.

The corresponding time-dependent finite difference solutions were obtained numerically by solving a periodic initial value problem. After a sufficiently long time from the beginning of calculations, numerical solutions over the ridge approach steady states with and without jumps. The numerical results clearly demonstrate the conclusions of the analytical study of the various features of flow over the ridge.

The fact that a lee side jump occurs for a relatively low Froude number of the flow upstream of a ridge may help to explain the not infrequent occurrence of strong wind situations (chinooks) along the eastern slope of the Rocky Mountains.

Since the present model treats a single layer of fluid, it does not permit a study of the vertical extent of jumps associated with the

ridge. For this reason, the present study is being extended to that of a two-layer model. By assigning different values of the densities and the flow velocities of the upper and lower fluids, it is possible to investigate the effects of thermal stratification and wind shear upon the formation and structure of hydraulic jumps. This will be discussed in a later article.

Acknowledgements

The authors wish to express their gratitude to Eugene Isaacson, Courant Institute of Mathematical Sciences, New York University, for his helpful comments and advice throughout this study. Samuel Burstein of the same institute suggested the use of the momentum form of the equations for numerical computations of jumps. Acknowledgement is also due Oleg Vasiliev, Director of the Institute of Hydrodynamics, Novosibirsk, U.S.S.R., who suggested the use of the rarefaction wave condition. Mention must also be made of the work of Larry Larsen, Johns Hopkins University, which became known to the authors during the study. He considered some aspects of shallow water flow over an obstacle, but his interests are somewhat different from the treatment in this article. Larry Williams and Joyce Takamine assisted in performing the numerical computations on the CDC 3600 and 6600 at the National Center for Atmospheric Research. Some numerical calculations were carried out on the CDC 6600 at the AEC Computing and Applied Mathematics Center of the Courant Institute of Mathematical Sciences, New York University.

Bibliography

[1] Alaka, M. A. (Editor), The airflow over mountains, Technical Notes No. 34, World Meteorological Organization, Geneva, 1960, 135 pp.

[2] Burstein, S. Z., Numerical methods in multidimensional shocked flows, AIAA Journal, Vol. 2, 1964, pp. 2111-2117.

[3] Chao, J. P., Chang, K. K., and Yan, S. M., A preliminary investigation on the formation of pressure jump produced by mountains in a two-layer model, Scientia Sinica, Vol. 15, 1966, pp. 723-729.

[4] Courant, R., Methods of Mathematical Physics, Vol. II, Partial Differential Equations, Interscience Publishers, New York, 1962, 830 pp.

[5] Holmboe, J., and Klieforth, H., Investigations of mountain lee waves and the air flow over the Sierra Nevadas, Final Report, Contract No. AF 19(604)-728, 1957, 290 pp.

[6] Kuettner, J., The rotor flow in the lee of mountains, GRD Research Notes No. 6, Geophys. Res. Directorate, Air Force Cambridge Res. Center (ASTIA Document No. AD 208862) 1959, 20 pp.

[7] Lax, P. and Wendroff, B., Systems of conservation laws, Comm. Pure Appl. Math, Vol. 13, 1960, pp. 217-237.

[8] Long, R. R., Some aspects of the flow of stratified fluids II, Experiments with a two-fluid system, Tellus, Vol. 6, 1954, pp. 97-115.

[9] McClain, P. E., Synoptic investigation of a typical chinook situation in Montana, Bull. Amer. Meteor. Soc., Vol. 33, 1952, pp. 87-94.

[10] Stoker, J. J., Water Waves, Interscience Publishers, New York, 1957, 567 pp.

Figure Legends

Fig. 1 A cross section view of the one layer model. The physical variables are defined in the text.

Fig. 2a M as a function of U as given by Eq. (3.4) for $F_o = 0.3$.

Fig. 2b M as a function of U as given by Eq. (3.4) for $F_o = 2.0$.

Fig. 3 Classification of asymptotic flow conditions as a function of the initial flow speed, F_o, and maximum height of the ridge, M_c. The crossed circles labeled A, B, C, and D show different cases of the numerical experiments described in Section 4.

Fig. 4 Upstream asymptotic conditions for domain II.

Fig. 5 Downstream asymptotic conditions for domain II.

Fig. 6 Contour lines of D_A and $\mathcal{F}_A$ in domain II as a function of F_o and M_c.

Fig. 7 Contour lines of C_ℓ.

Fig. 8 Contour lines of Φ_c and $\mathcal{F}_c$ at the ridge crest.

Fig. 9 Contour lines of C_r for domain IIb and M^* for IIa.

Fig. 10 Downstream asymptotic conditions for domain IIa.

Fig. 11 Contour lines of D_X and $\mathcal{F}_X$.

Fig. 12 Contour lines of D_B and $\mathcal{F}_B$ for domain IIb and those of Φ_- and $\mathcal{F}_-$ for domain IIa.

Fig. 13 Contour lines of $\tilde{D}_+$ and $\mathcal{F}_+$ for domain IIa.

Fig. 14a Numerical results for Case A after 1000 time steps. Height and velocity are shown in the dimensionless units used in the text. The time is in units of seconds.

Fig. 14b Numerical results for Case B after 400 time steps.

Fig. 14c Numerical results for Case C after 400 time steps.

Fig. 14d Numerical results for Case D after 1000 time steps.

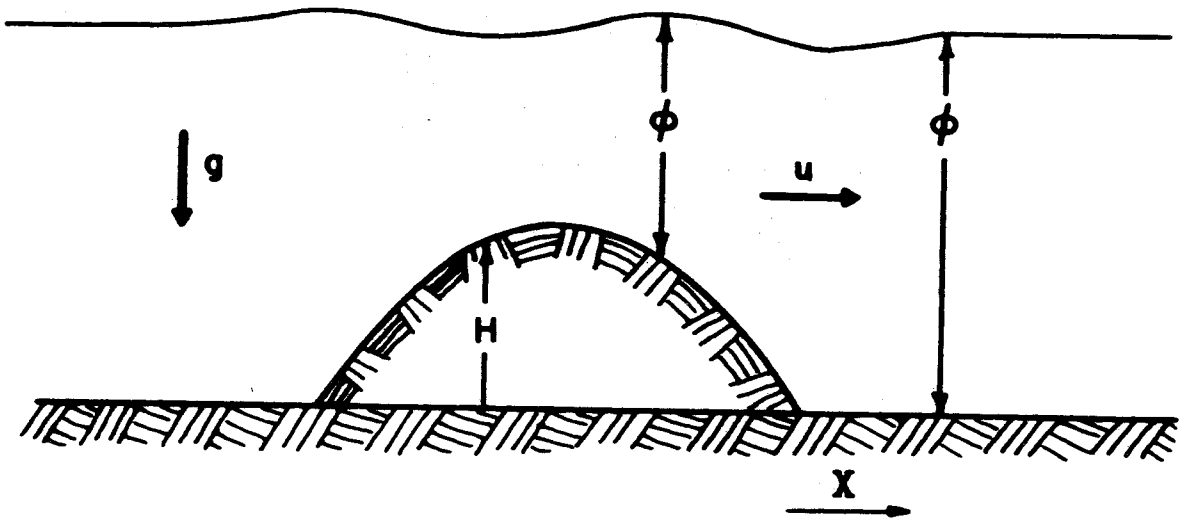

Fig. 1 A cross section view of the one layer model. The physical variables are defined in the text.

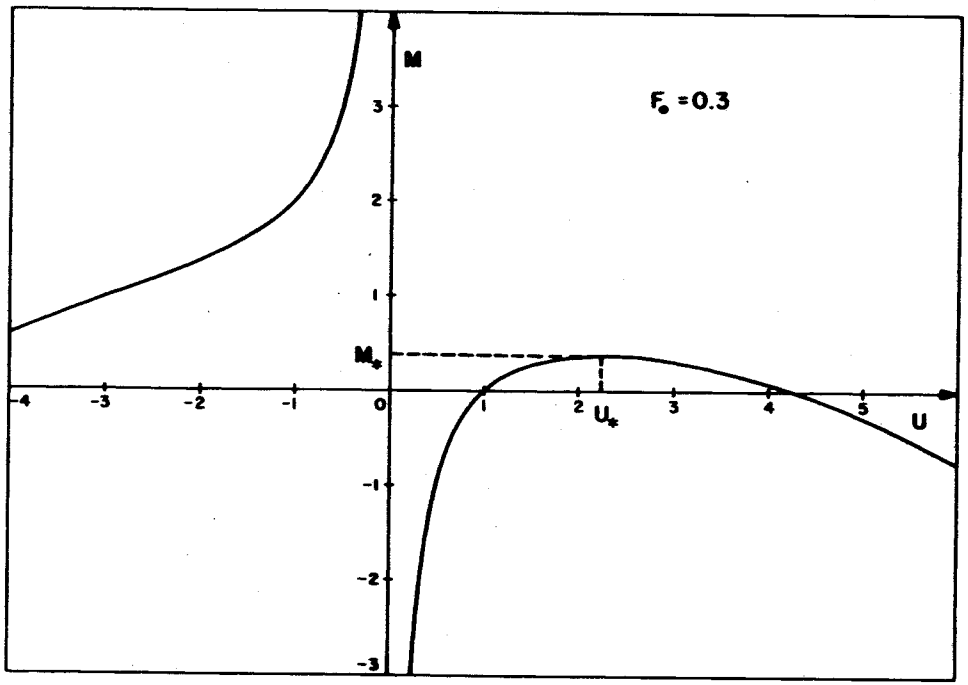

Fig. 2a M as a function of U as given by Eq. (3.4) for $F_o = 0.3$.

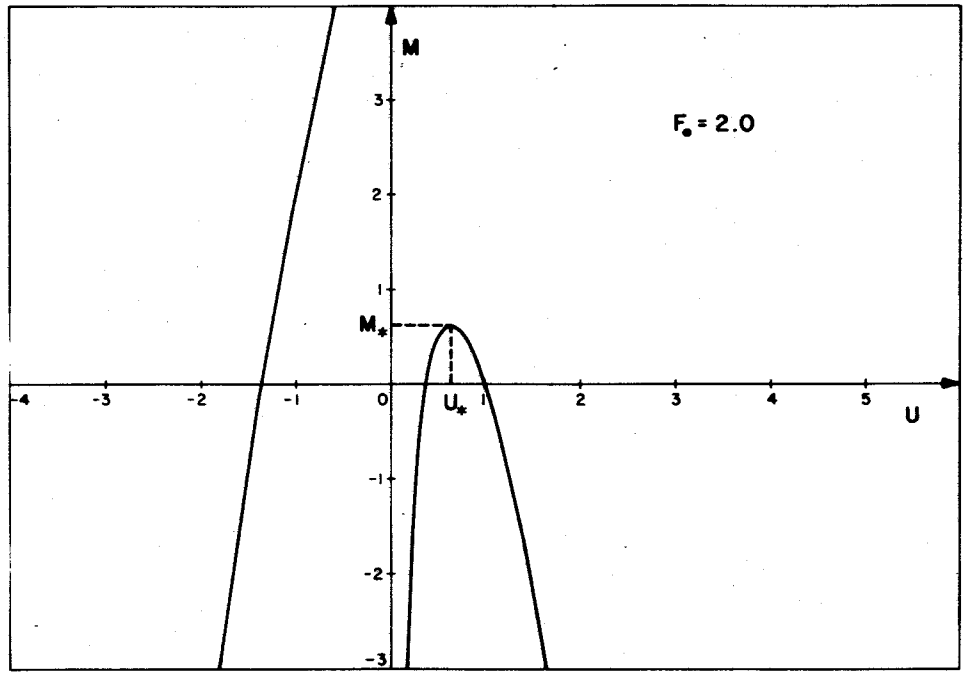

Fig. 2b M as a function of U as given by Eq. (3.4) for F_o = 2.0.

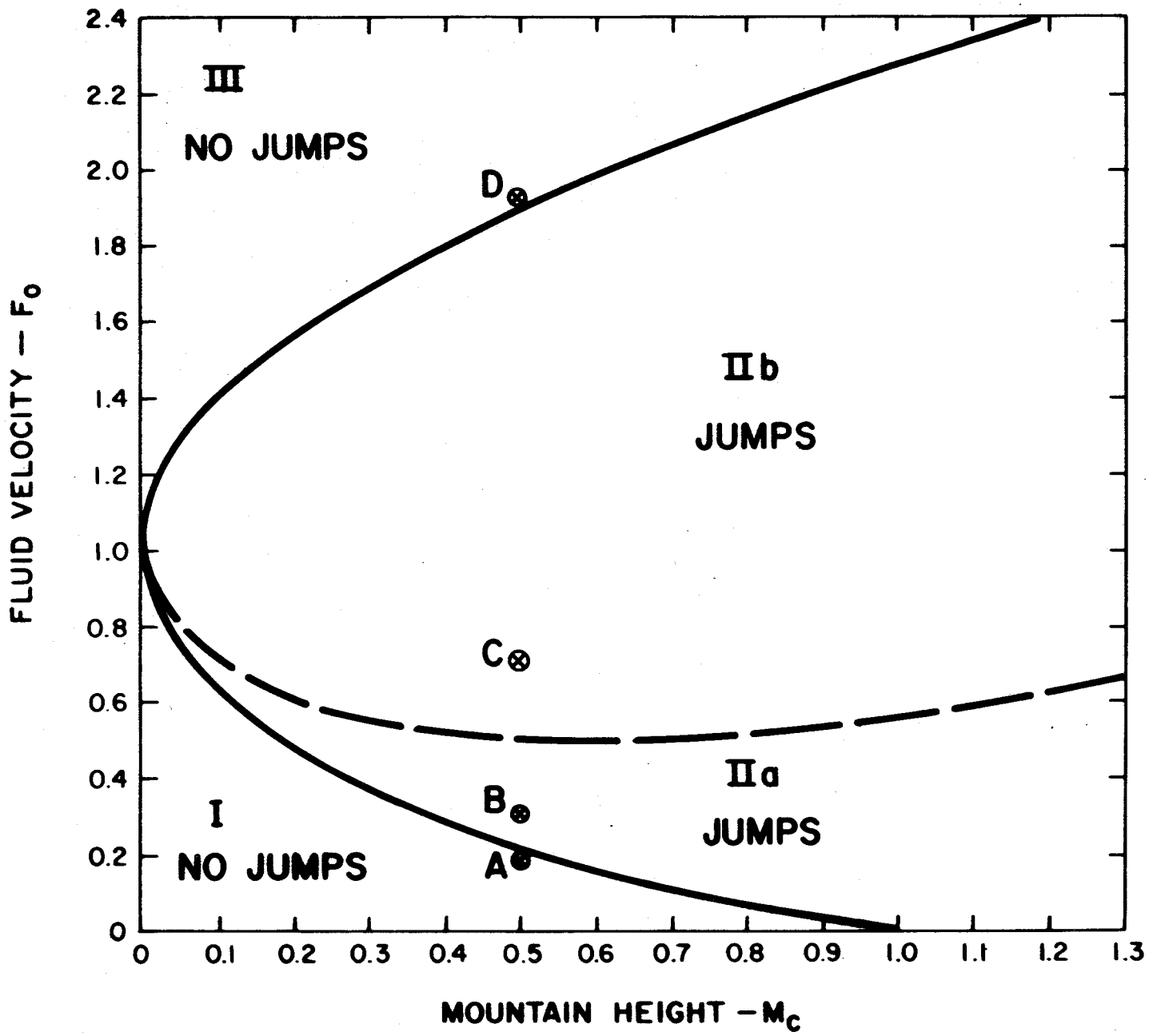

Fig. 3 Classification of asymptotic flow conditions as a function of the initial flow speed, F_o, and maximum height of the ridge, M_c. The crossed circles labeled A, B, C, and D show different cases of the numerical experiments described in Section 4.

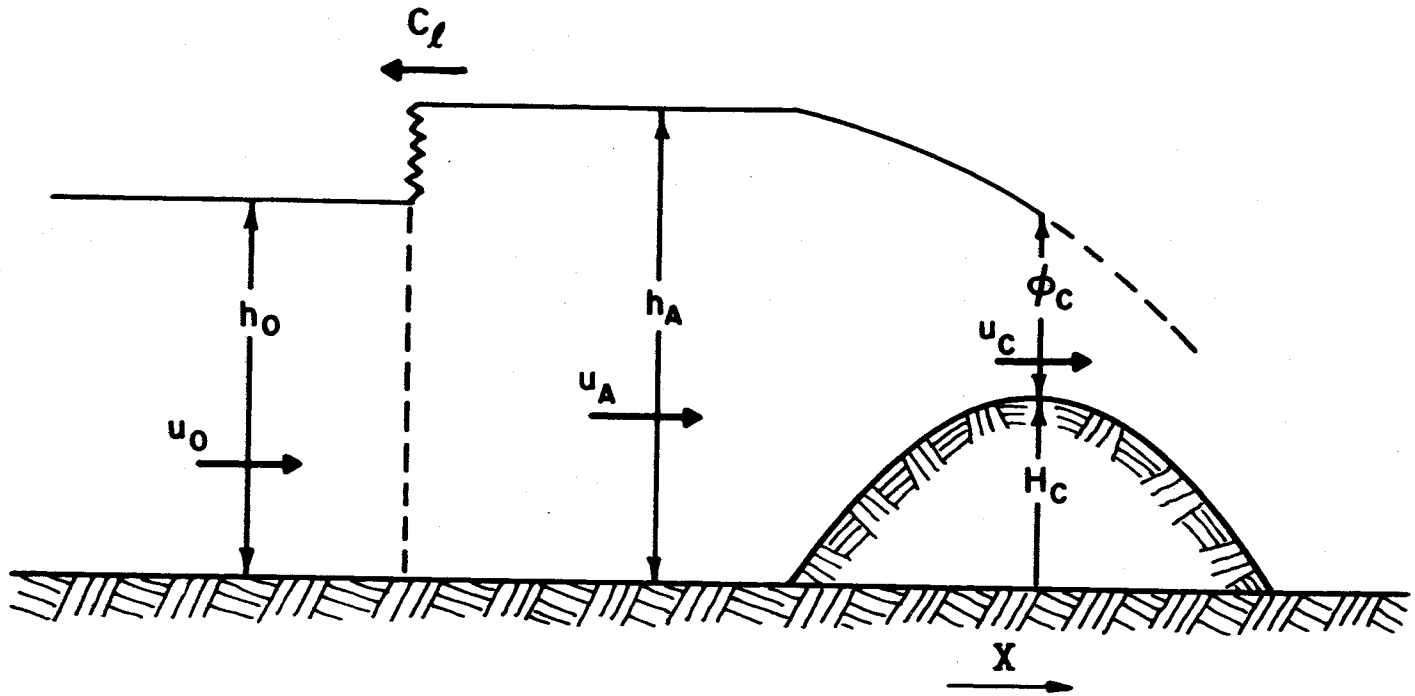

Fig. 4 Upstream asymptotic conditions for domain II.

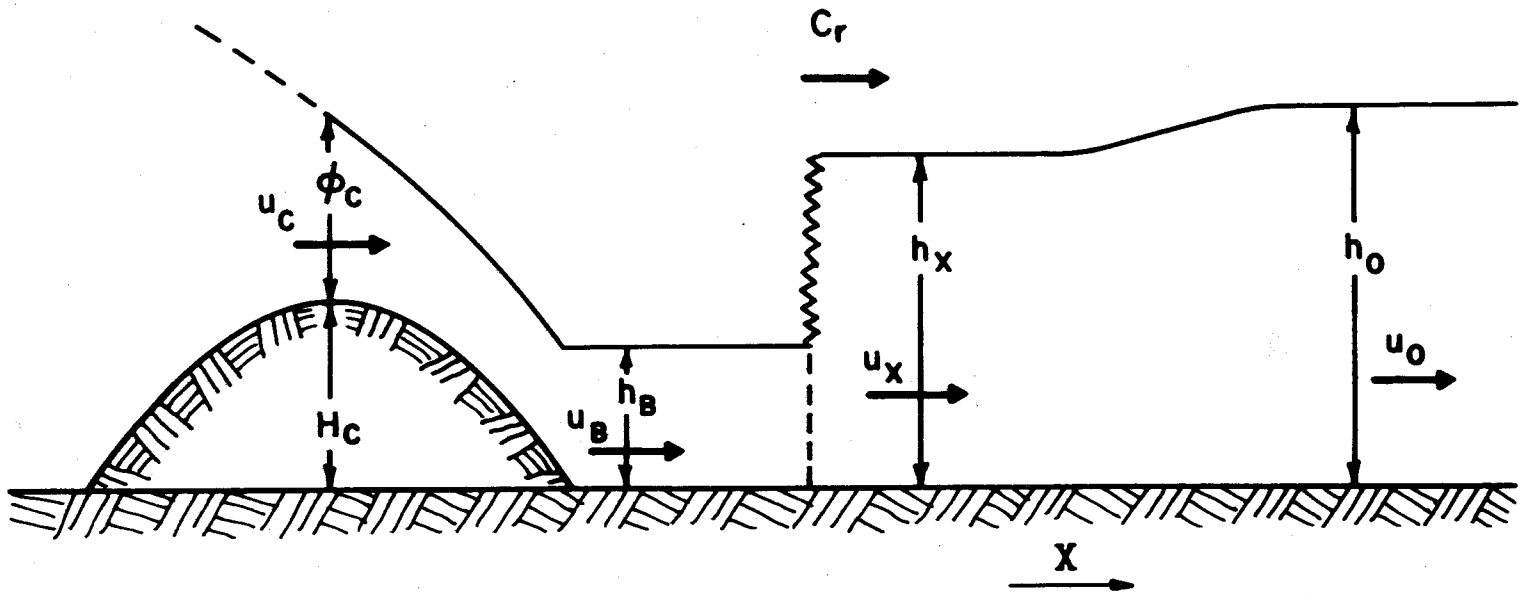

Fig. 5 Downstream asymptotic conditions for domain II.

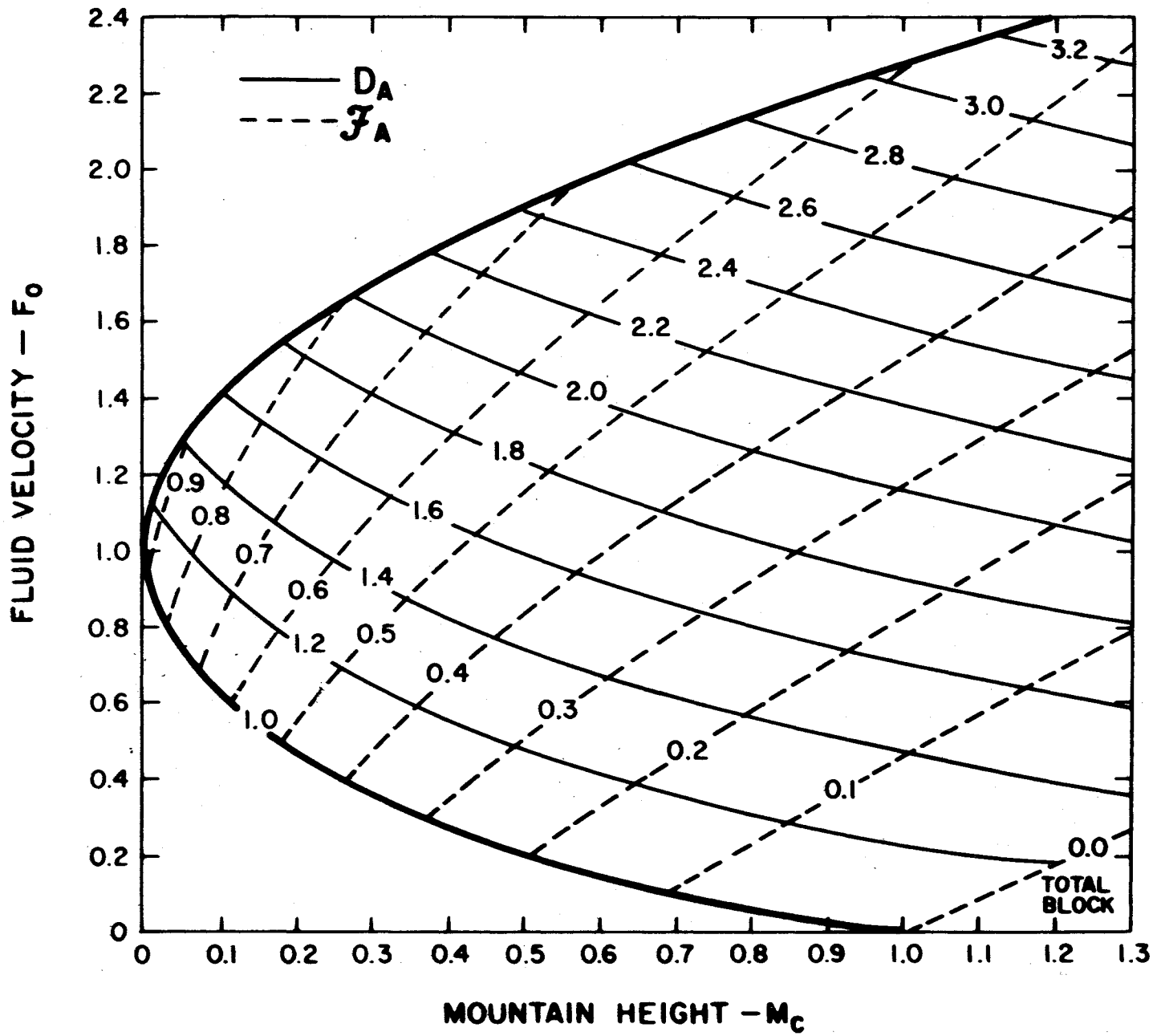

Fig. 6 Contour lines of D_A and $\mathcal{F}_A$ in domain II as a function of F_o and M_c.

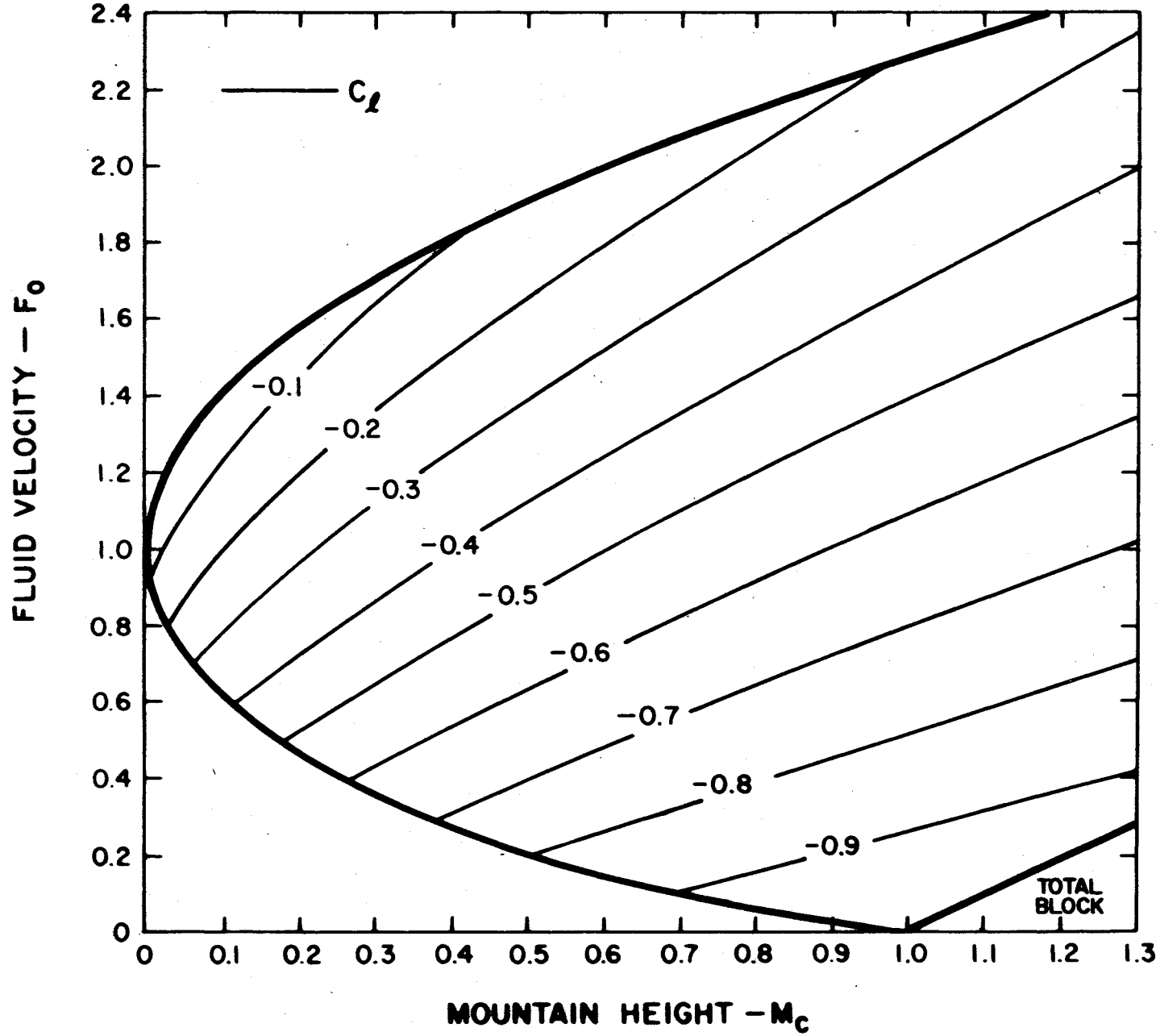

Fig. 7 Contour lines of C_ℓ.

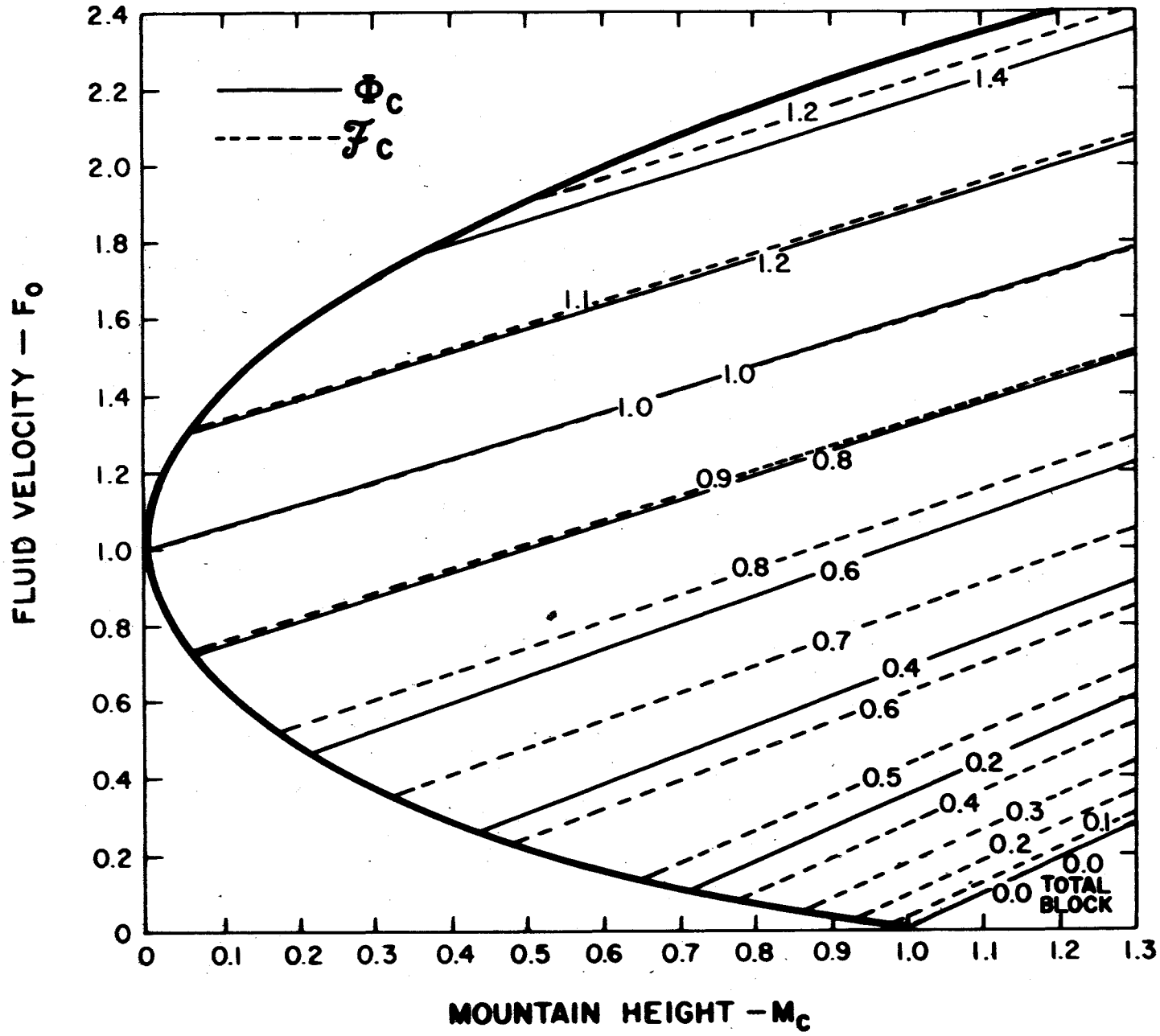

Fig. 8 Contour lines of Φ_c and $\mathcal{F}_c$ at the ridge crest.

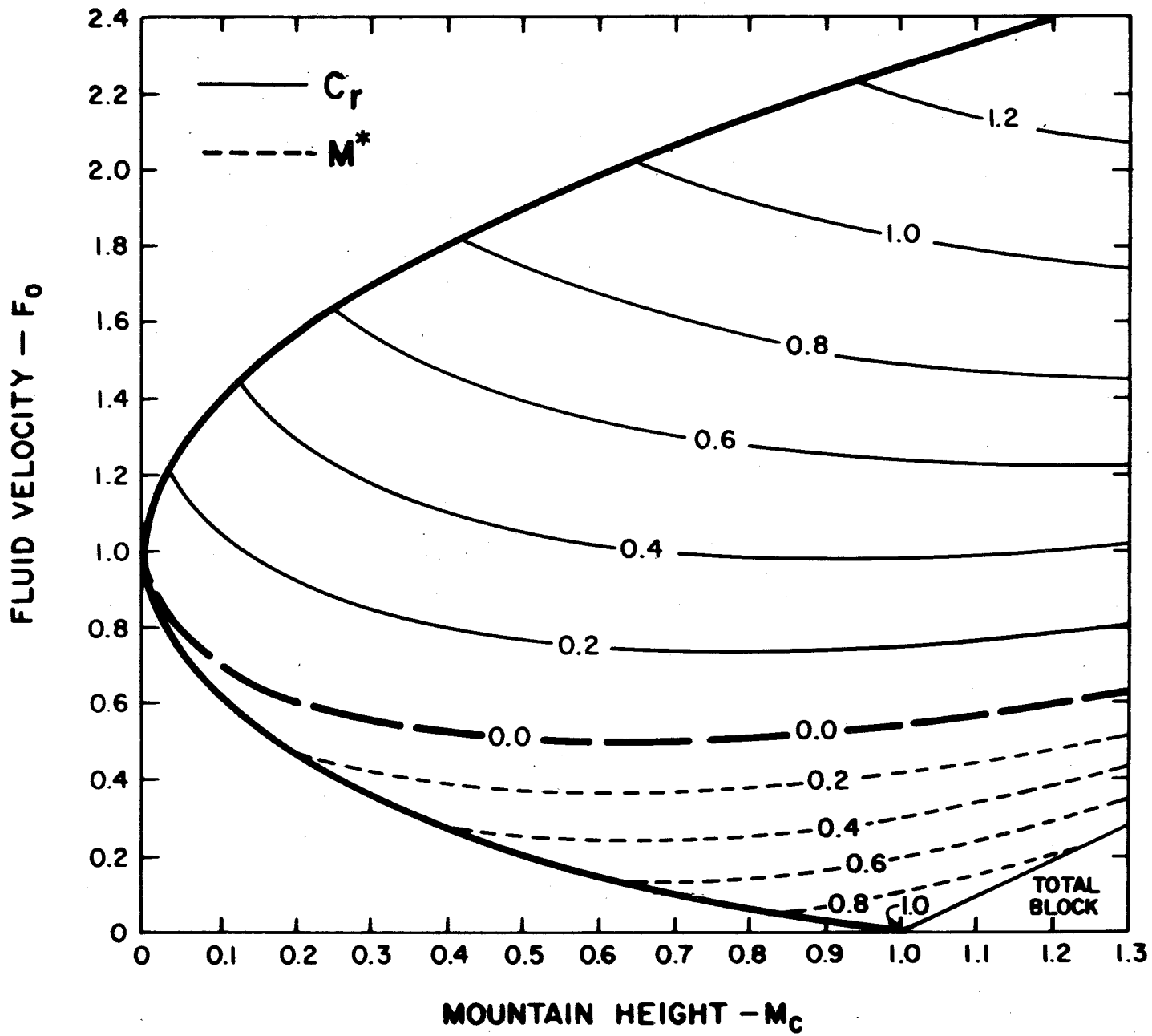

Fig. 9 Contour lines of C_r for domain IIb and M^* for IIa.

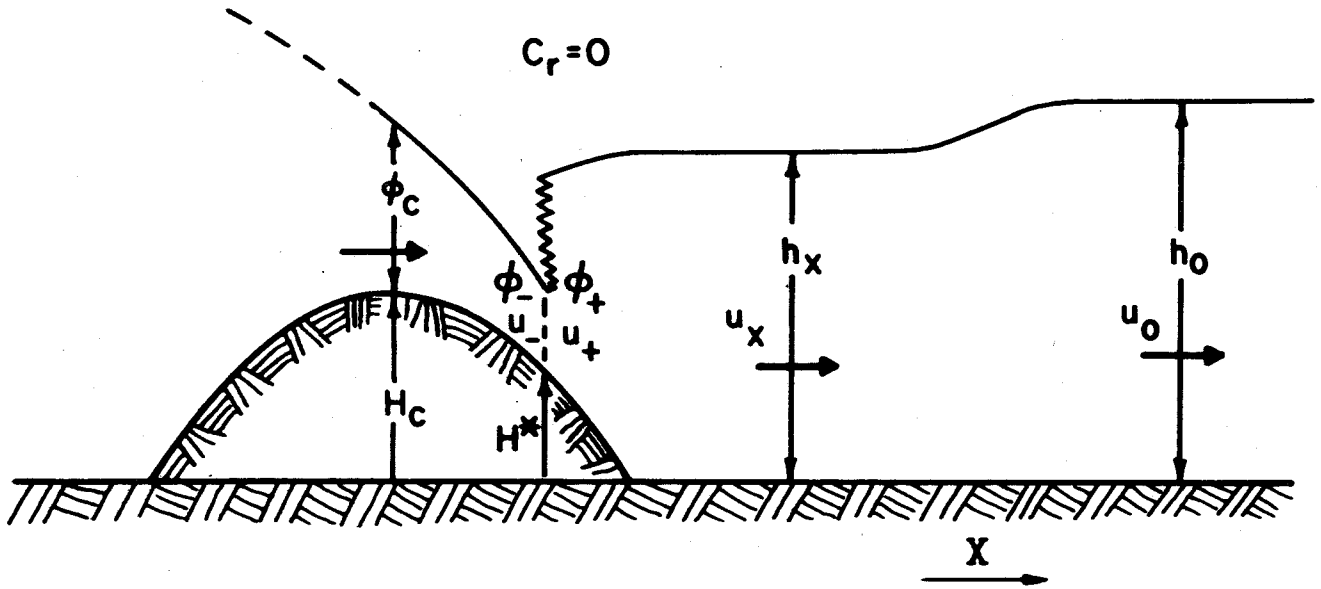

Fig. 10 Downstream asymptotic conditions for domain IIa.

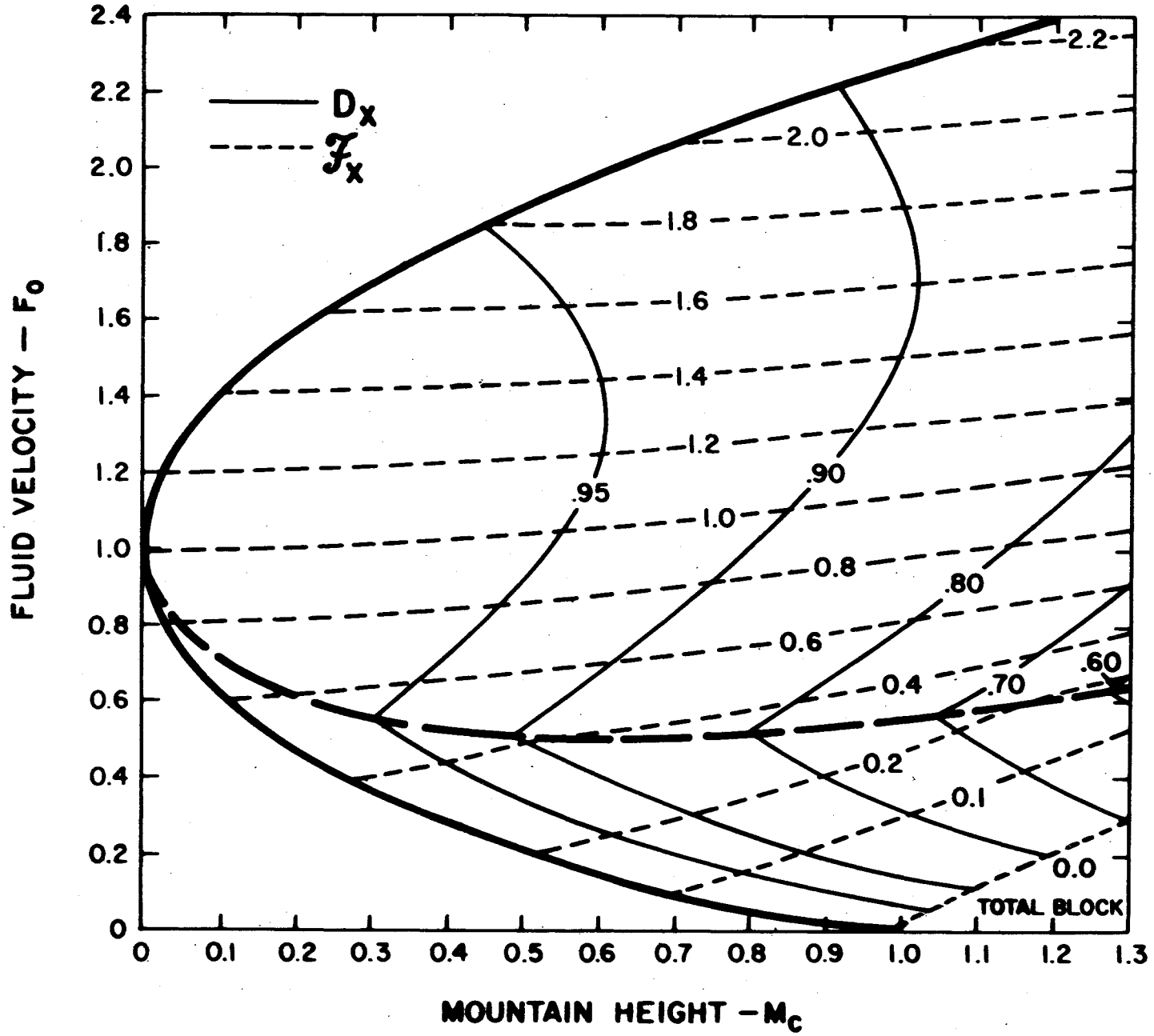

Fig. 11 Contour lines of D_x and $\mathcal{F}_x$.

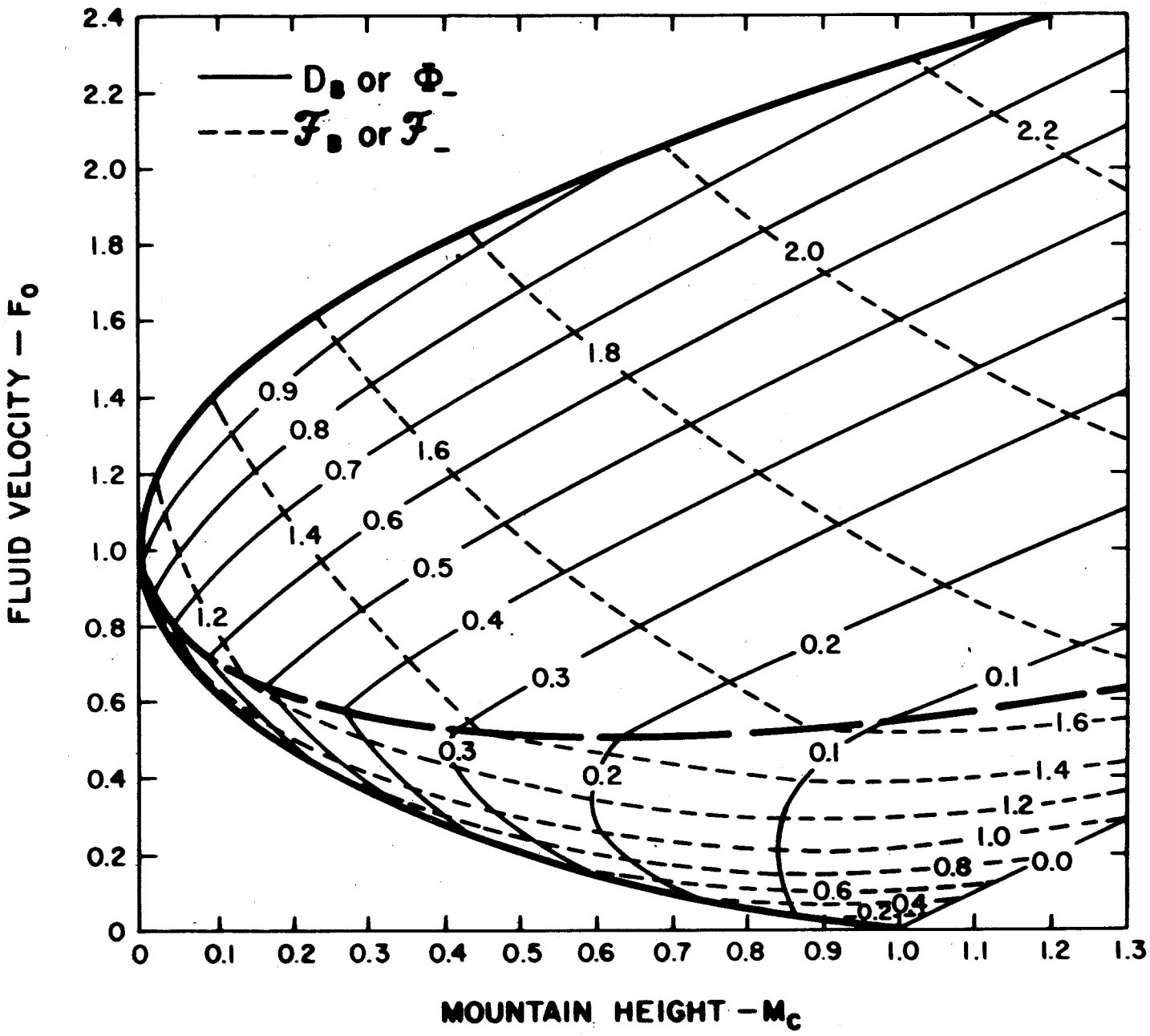

Fig. 12 Contour lines of D_B and $\mathcal{F}_B$ for domain IIb and those of Φ_- and $\mathcal{F}_-$ for domain IIa.

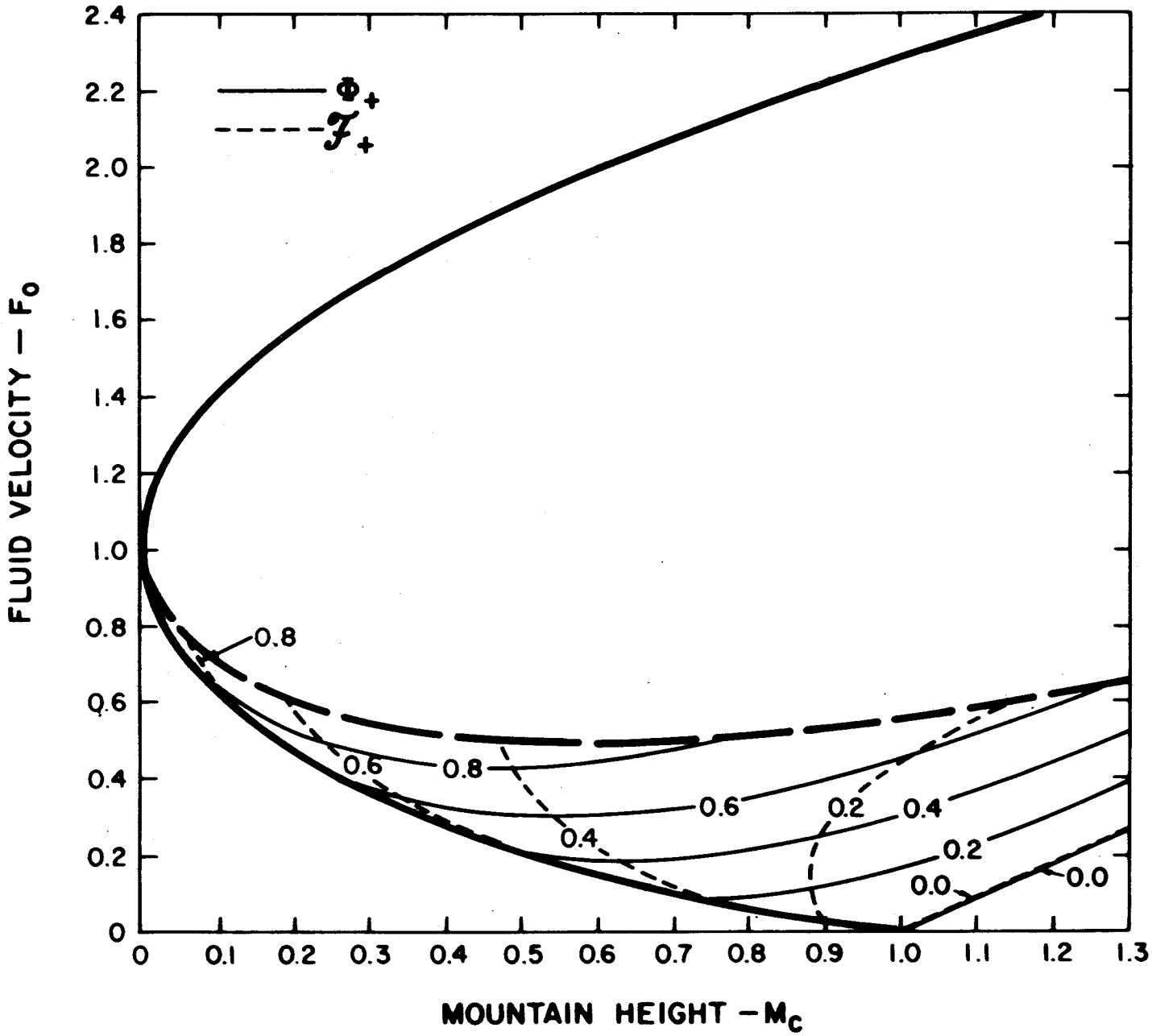

Fig. 13 Contour lines of Φ_+ and $\mathcal{F}_+$ for domain IIa.

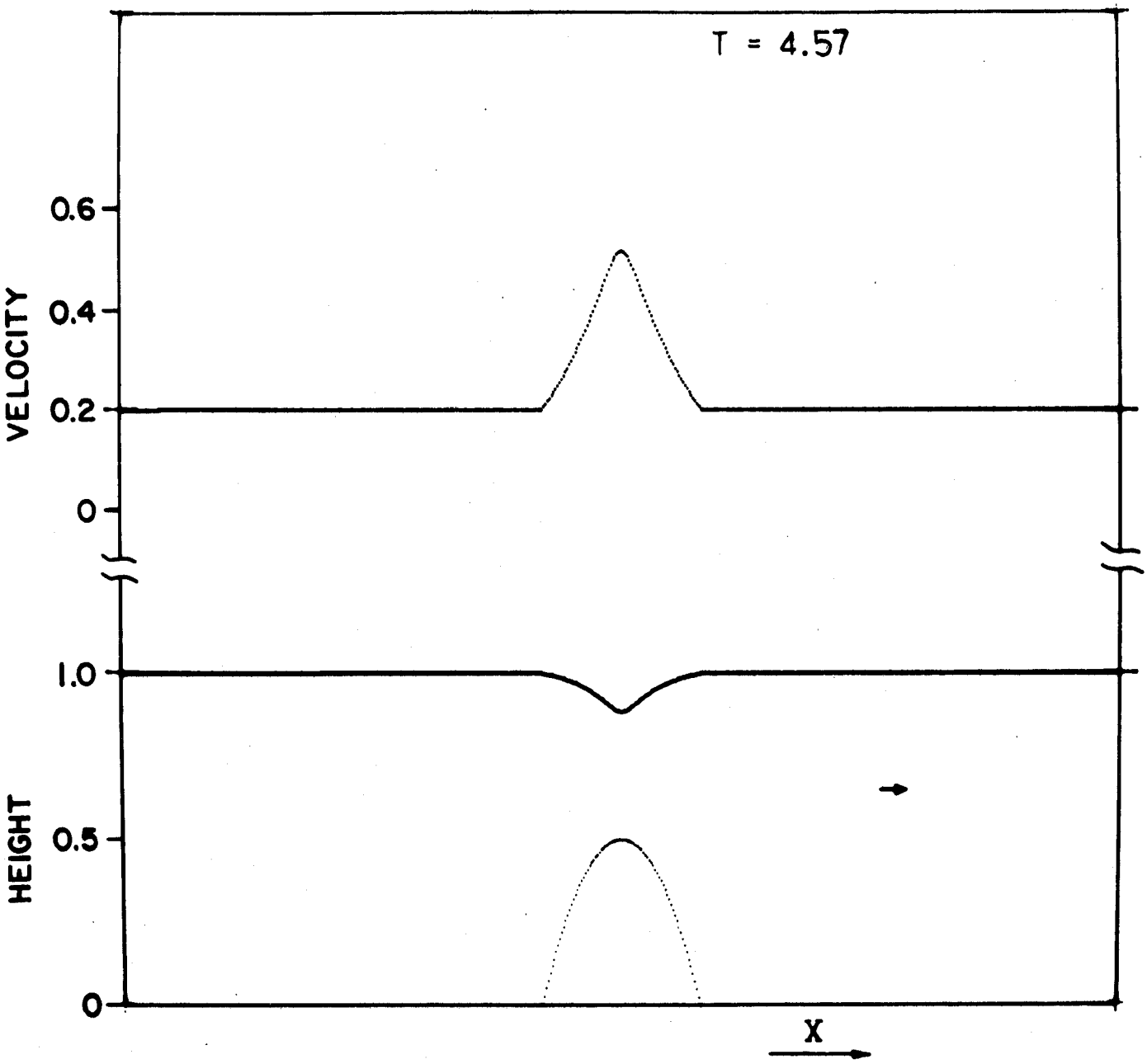

Fig. 14a Numerical results for Case A after 1000 time steps. Height and velocity are shown in the dimensionless units used in the text. The time is in units of seconds.

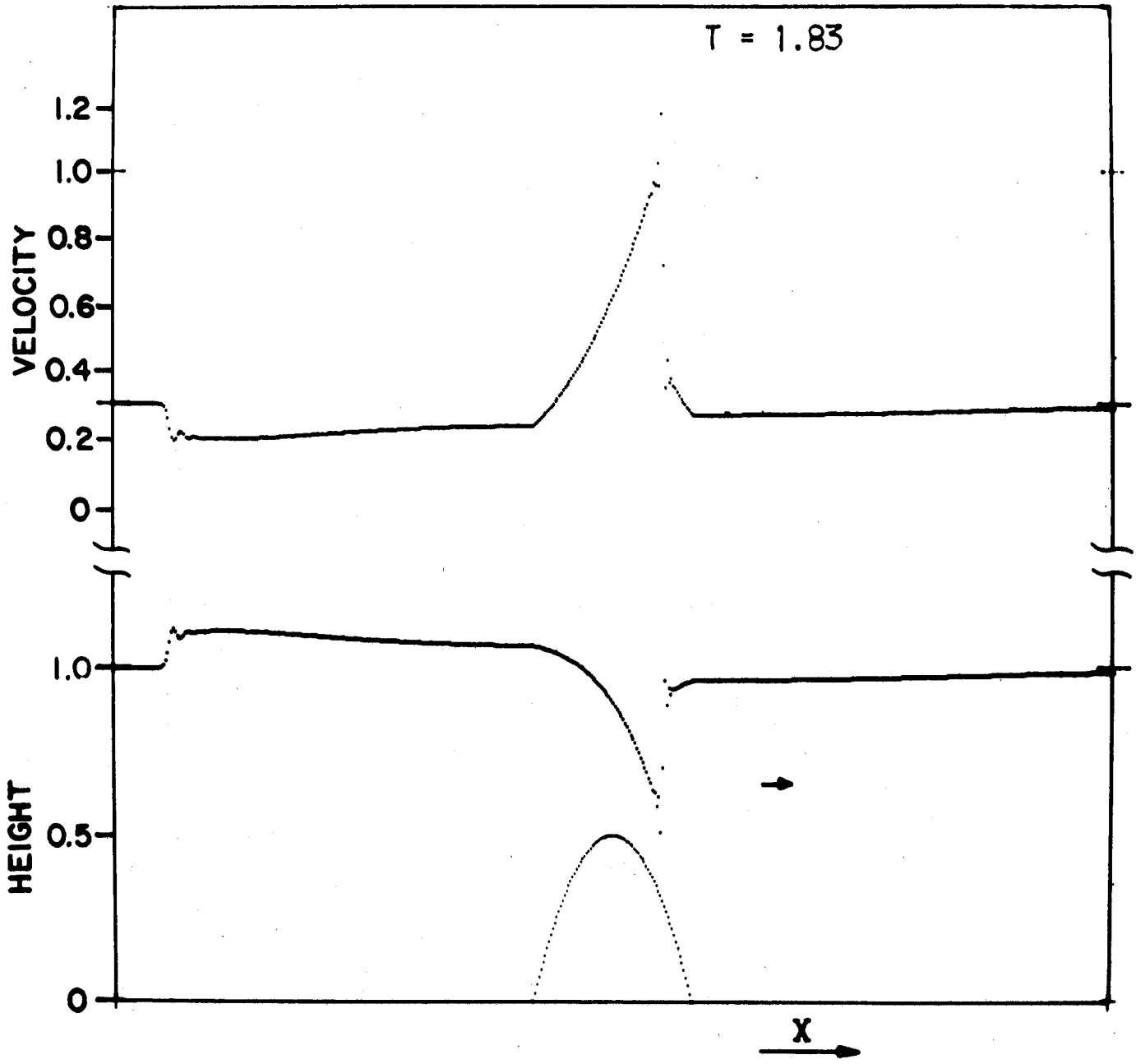

Fig. 14b Numerical results for Case B after 400 time steps.

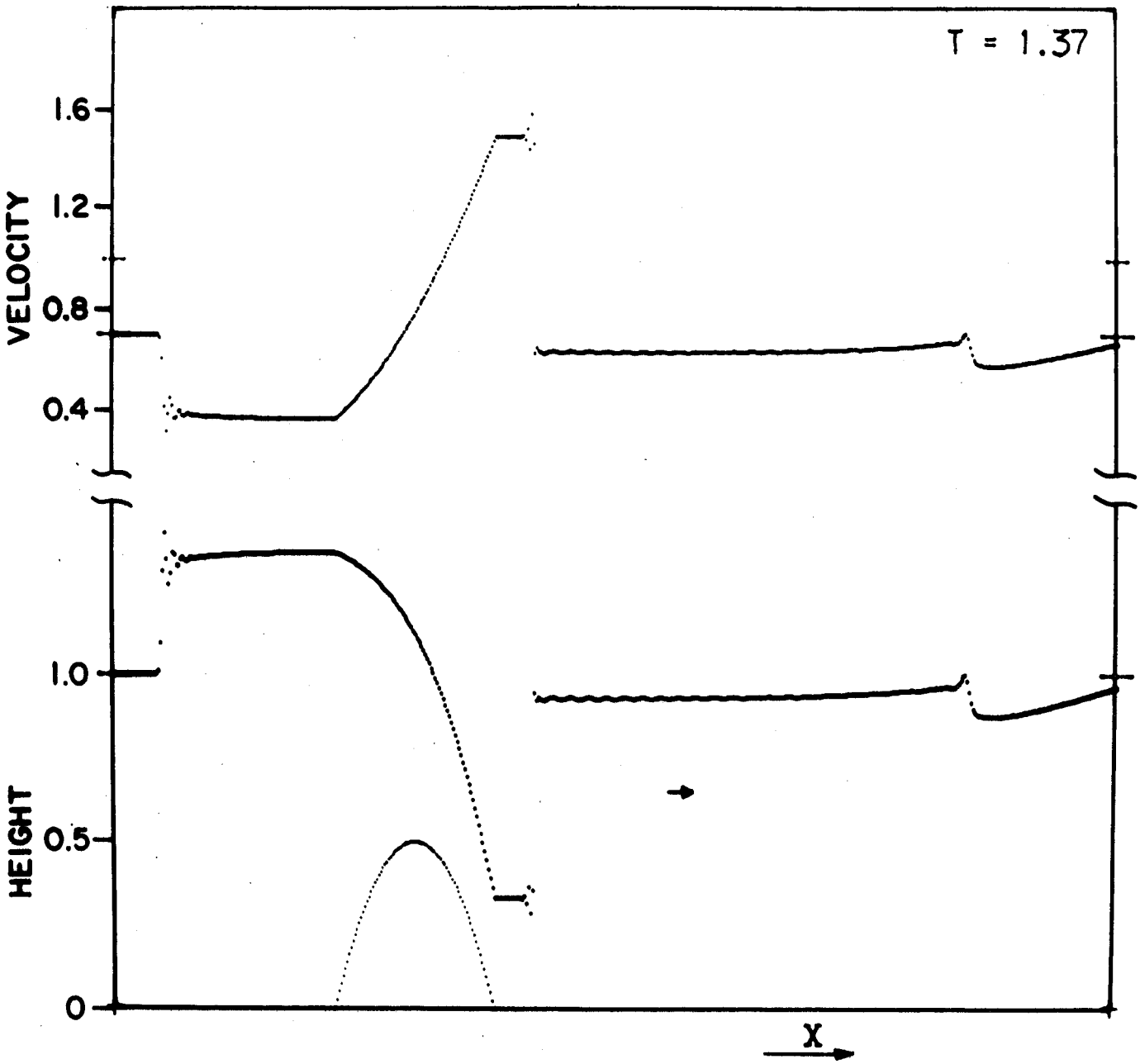

Fig. 14c Numerical results for Case C after 400 time steps.

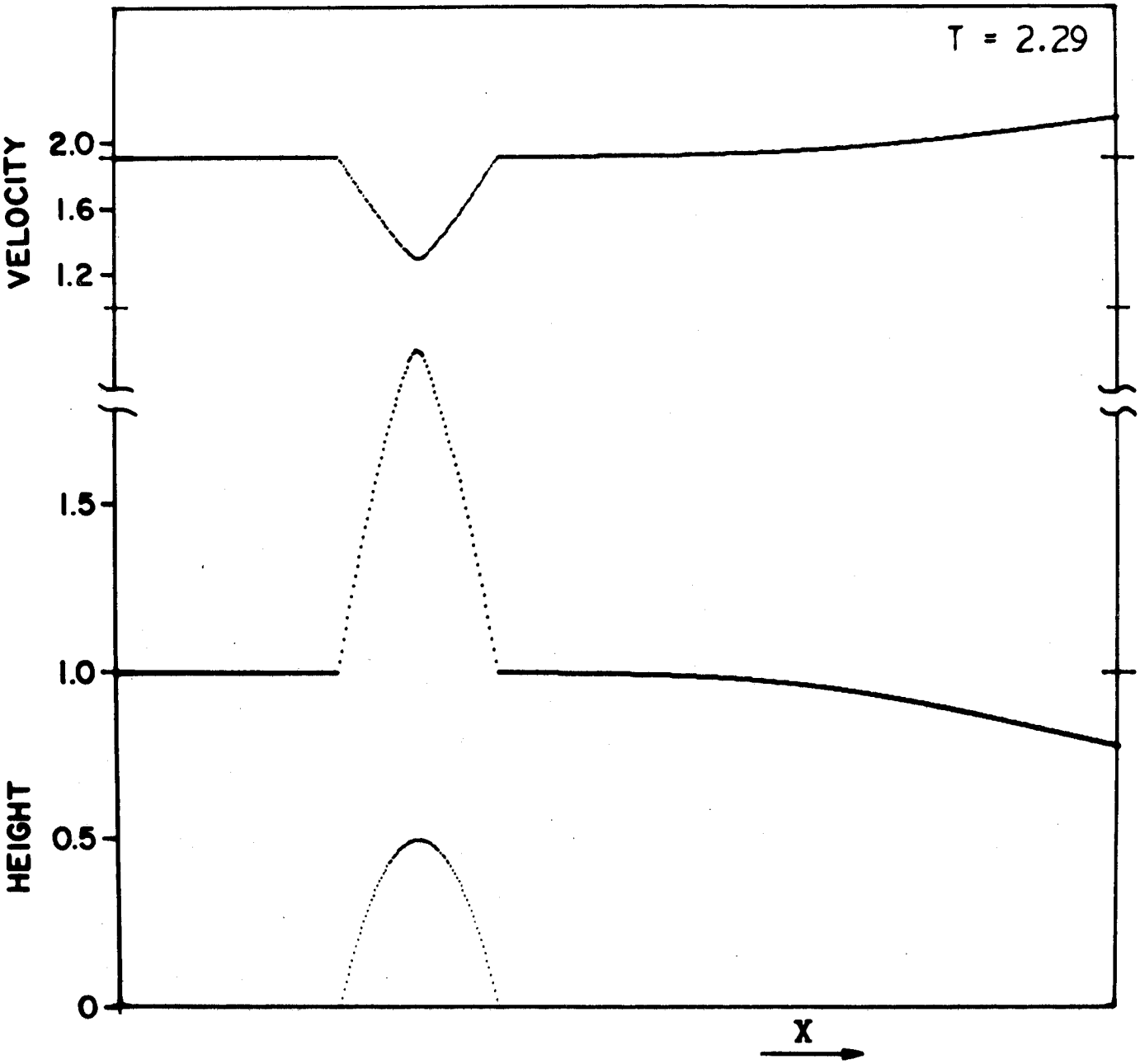

Fig. 14d Numerical results for Case D after 1000 time steps.